Kinetic Modeling for Methane Reforming with Carbon Dioxide over a Mixed-Metal Carbide Catalyst

Mahesh V. Iyer,† Lawrence P. Norcio, Edwin L. Kugler, and Dady B. Dadyburjor*

Department of Chemical Engineering, West Virginia University, P.O. Box 6102, Morgantown, West Virginia 26506-6102

A cobalt−tungsten η-carbide material [Co_6W_6C] was investigated as a precursor for a stable and active catalyst for the dry reforming of methane to produce synthesis gas. The kinetics of CH_4/CO_2 reforming were studied under differential conditions over a temperature range of 500−600 °C, based on a detailed experimental design. The observed rates qualitatively follow a Langmuir−Hinshelwood type of reaction mechanism. Such a scheme is considered quantitatively, with four reactions: methane reforming, reverse water-gas shift, carbon deposition, and carbon removal by a reverse Boudouard reaction. Of these, carbon deposition and carbon removal are generally disregarded in most of the reported kinetic models. The parameters of the model were successfully estimated for all of the experimental data. The comparison plots of the observed data and the predicted model show generally a good fit for all of the product species.

Introduction

Methane is a major component (70−98%) of natural gas, reserves of which are abundant worldwide.[1] Existing industrial processes use methane as a primary feedstock for synthesis gas (syngas), a mixture of carbon monoxide and hydrogen, which serves as the feedstock for a variety of downstream processes:[2−6] methanol synthesis, Fischer−Tropsch synthesis, ammonia synthesis, etc. Methane is also an unavoidable byproduct in the Fischer−Tropsch process. Reducing the cost of syngas produced from natural gas and reconverting Fischer−Tropsch methane back to syngas would play significant roles in the economics of the production of synthetic liquid fuels and chemicals.

Reforming of methane to syngas can be carried out in four different ways:[2,3,5,7,8] partial oxidation, autothermal reforming, steam reforming, and dry reforming. Of these, partial oxidation uses oxygen directly

$$CH_4 + {}^1/_2O_2 \rightarrow CO + 2H_2 \quad (1)$$

autothermal reforming uses oxygen and steam

$$3CH_4 + H_2O + O_2 \rightarrow 3CO + 7H_2 \quad (2)$$

while steam reforming

$$CH_4 + H_2O \rightarrow CO + 3H_2 \quad (3)$$

is the conventional process and produces syngas with high H_2/CO ratios. Dry reforming, using carbon dioxide in place of water

$$CH_4 + CO_2 \rightarrow 2CO + 2H_2 \quad (4)$$

has been proposed as a promising technology because of the use of the greenhouse gas CO_2. Besides, dry reforming can be employed in those natural-gas fields where there is an abundance of CO_2.[7,9] Dry reforming can also be used with a Fischer−Tropsch recycle stream, which would also contain CO_2. Finally, dry reforming has been evaluated[3] to have the lowest operating costs, about 20% lower than those of the other reforming processes.

Metal catalysts are suitable for dry reforming, with nickel-based catalysts preferred commercially over noble metals, because of the inherent availability and low costs of the former. However, nickel also catalyzes the formation of coke, unsaturated polyaromatic hydrocarbons with H/C ratios less than unity, via methane decomposition and/or CO disproportionation.[2,3,5,7] Coke may form on the catalyst surface and/or the tubes of the reformer and leads to deactivation of the catalyst and plugging of the tubes. Hence, coke formation is one of the major problems associated with dry reforming using these catalysts.[3,6]

There has been considerable interest in the catalytic properties of metal carbides. The precursors for these metal carbides are abundant and, hence, they may be effective enough to replace noble metals as catalysts.[5,9] Carbides of molybdenum and tungsten, in particular, have gained attention in recent years for various reactions.[5,9] Several groups have reported using these metal carbide catalysts for dry reforming of methane.[9−13] These carbides are stable at elevated pressures and are moderately resistant to carbon deposition (CD). However, addition of a second metal could result in improvements in activity and stability.

Recently, we have shown[14] that a catalyst obtained by the appropriate pretreatment of a cobalt−tungsten η-carbide [Co_6W_6C] is active for dry reforming. Conversions are high, H_2/CO ratios approach unity, and the catalyst is stable for at least 150 h. The stable form of the catalyst is believed to be a solid mixture of WC + Co + C. Coke formation does not lead to deactivation of this type of catalyst, unlike the conventional metal catalysts. Hence, the presence of carbon is believed to be integral to the performance of the catalyst.

In the present work, kinetic models have been developed for the carbon dioxide reforming of methane over

* To whom correspondence should be addressed. Tel.: (304) 293-2111 ext. 2411. Fax: (304) 293-4139. E-mail: dady.dadyburjor@mail.wvu.edu.

† Present address: Department of Chemical Engineering, The Ohio State University, Columbus, OH 43210.

10.1021/ie020677q CCC: $25.00
Published on Web 04/29/2003

the stable catalyst prepared from the η-carbide precursor, using a set of designed experiments. The experiments were performed under differential reaction conditions and were designed to show dependencies on partial pressures of the reactants and on temperatures between 500 and 600 °C. A Langmuir−Hinshelwood (LH) type of mechanism has been shown to be useful in interpreting the data.

Existing Models for Dry Reforming. (a) Power-Law Models. There have been various reports[4,6,15−19] in which the dry-reforming kinetics and the rate expressions have been approximated by a simple power-law equation:

$$r = kP_{CH_4}{}^{m}P_{CO_2}{}^{n} \tag{5}$$

The values of the power-law rate coefficient k and the indices m and n vary for various catalyst systems. The advantage of these models is their simplicity in application and determination. However, these models are inadequate over a wider range of partial pressure data.

(b) Mechanisms. There have been various stepwise mechanisms proposed for the dry-reforming reaction between CO_2 and CH_4.[4−7,20−32] We report on mechanisms suggested over three basic types of catalysts: supported nickel, supported noble metal, and carbide catalysts.

On the basis of their investigation of a Ni/SiO_2 catalyst using isotopic transient experiments combined with in situ DRIFT spectroscopy techniques, Kroll et al.[26] propose three basic mechanistic steps: methane activation, carbon dioxide activation, and water formation. The rate-determining step was proposed to be the reaction of adsorbed C and adsorbed O to form CO:

$$C^* + O^* \rightleftarrows CO + 2^* \tag{6}$$

Here * indicates an adsorption site and I* indicates adsorbed species I.

Efstathiou et al.[24] investigated dry reforming over Rh catalysts supported on yttria-stabilized zirconia (YSZ) and Al_2O_3 using steady-state tracer techniques. Their experiments indicate that the sites occupied by C species derived from CH_4 are of a different nature than those occupied by C species derived from CO_2, with the former having a greater reactivity toward oxygen or OH species.

For supported Pt and Ni catalysts, Bradford and Vannice[27,28] propose that the dissociation of CH_xO species to CO and H

$$CH_xO \rightarrow CO + xH \tag{7}$$

is rate determining. Osaki et al.[23,29] and Luo et al.[32] make similar assertions, based on their studies over supported Ni catalysts. Further, CH_4-CO_2 pulsing experiments[32] indicate an absence of CH_x species on the catalyst surfaces, suggesting that the interaction of CH_x species with surface oxygen is fast, to give the CH_xO species via

$$CH_x + O \rightarrow CH_xO \tag{8}$$

Claridge et al.[5] propose that, for high-surface-area molybdenum and tungsten carbide catalysts, there are two possible competing, equally important, mechanisms for dry reforming. One of these is the cycling (or redox) mechanism, and the other is the noble-metal-type mechanism. In the former mechanism, CO_2 adsorbs dissociatively to CO and O*. The O* formed reacts with the carbon on the carbide surface (C_s) to leave a vacancy ($^{\square}$). This vacancy is then filled with either C* from carbon adsorbed from methane, giving back the carbide, or O* to oxidize the metal carbide to the oxide. These steps can be given as

$$CO_2 + * \rightleftarrows CO + O^* \tag{9a}$$

$$WC_s + O^* \rightleftarrows W^{\square} + CO \tag{9b}$$

$$W^{\square} + C^* \rightleftarrows WC_s \tag{9c}$$

$$W^{\square} + O^* \rightleftarrows WO\ (\text{oxides}) \tag{9d}$$

In the noble-metal-type mechanism, the O* from the dissociation of CO_2 reacts with the C* formed from the dissociation of methane, instead of the carbon from the carbide. This mechanism can be given as

$$CH_4 + * \rightleftarrows C^* + 2H_2 \tag{9e}$$

$$CO_2 + * \rightleftarrows CO + O^* \tag{9f}$$

$$O^* + C^* \rightleftarrows CO \tag{9g}$$

(c) Competing Reactions. The overall reaction for dry reforming (eq 4) occurs in parallel and series with other competing reactions. When eq 4 has been included for completeness, a set of possible reactions has been written as[33]

$$CH_4 + CO_2 \rightleftarrows 2CO + 2H_2 \quad \text{(methane reforming, MR)} \tag{10a}$$

$$CO_2 + H_2 \rightleftarrows CO + H_2O \quad \text{(reverse water-gas shift, RWGS)} \tag{10b}$$

$$CO_2 + 4H_2 \rightleftarrows CH_4 + 2H_2O \quad \text{(methanation)} \tag{10c}$$

$$CH_4 + H_2O \rightleftarrows CO + 3H_2 \quad \text{(steam reforming)} \tag{10d}$$

$$CH_4 \rightleftarrows 2H_2 + C \quad \text{(methane decomposition)} \tag{10e}$$

$$2CO \rightleftarrows CO_2 + C \quad \text{(Boudouard reaction)} \tag{10f}$$

$$C + H_2O \rightleftarrows CO + H_2 \quad \text{(coal gasification)} \tag{10g}$$

Several investigators have taken a few stoichiometrically independent reactions from these, coupled them with a LH, Hougen−Watson (HW), or Eley−Rideal (ER) type of rate expression, and come up with a kinetic rate expression to describe the reaction system. A detailed list of the rate expressions derived by various investigators is tabulated in Table 1. The advantages and disadvantages of each formulation are discussed elsewhere.[40]

The kinetic model used in the current work is described in detail in a later section. In brief, this model uses a few elementary steps, combined to comprise dry reforming in parallel with three other reactions: RWGS, methane decomposition, and the reverse Boudouard (RB) reaction, i.e., eq 10a,b,e and the reverse of eq 10f.

Experimental Section

Catalyst-Testing Unit. The catalyst testing unit is as shown in Figure 1 and is similar to that used by Liu et al.[41] The entire system is computer controlled using

Table 1. Proposed Rate Expressions for Dry Reforming of Methane with Carbon Dioxide

eq	rate model	catalyst	ref
11	$r_{ref} = \frac{k_{ref}P_{CH_4}(P_{CO_2} + P_{H_2O})}{[1 + 24(P_{CO_2} + P_{H_2O}) + 8P_{H_2}]^2}$	Cu/SiO_2	34
12	$r_{ref} = \frac{k_{ref}P_{CH_4}}{1 + a\frac{P_{H_2O}}{P_{H_2}} + bP_{CO}}$	Ni foil	20
13	$r_{ref} = \frac{k_{ref}K_{CH_4}K_{CO_2}P_{CH_4}P_{CO_2}}{(1 + K_{CH_4}P_{CH_4} + K_{CO_2}P_{CO_2})^2}$	Rh/Al_2O_3	17
14	$r_{ref} = \frac{aP_{CH_4}P_{CO_2}^{\ 2}}{(a + bP_{CO_2}^{\ 2} + cP_{CH_4})^2}$	Ni/Al_2O_3, $Ni/CaO-Al_2O_3$	35
15	$r_{ref} = \frac{k_{ref}\left(P_{CH_4} - \frac{P_{H_2}^{\ 2}P_{CO}^{\ 2}}{K_{ref}P_{CO_2}}\right)}{1 + \frac{P_{CO}^{\ 2}}{K_{R,C-z}P_{CO_2}}}$	Ir/Al_2O_3	25
16	$r_{ref} = \frac{k_{ref}K_{CH_4}\left(P_{CH_4}P_{CO_2} - \frac{P_{H_2}^{\ 2}P_{CO}^{\ 2}}{K_{ref}}\right)}{1 + K_{CH_4}P_{CH_4}}$	Ir/Al_2O_3	33
17	$r_{ref} = \frac{k_{ref}K_{CO_2}\left(P_{CH_4}P_{CO_2} - \frac{P_{H_2}^{\ 2}P_{CO}^{\ 2}}{K_{ref}}\right)}{1 + K_{CO_2}P_{CO_2}}$	Ir/Al_2O_3	33
18	$r_{ref} = \frac{k_{ref}K_{CH_4}K_{CO_2}\left(P_{CH_4}P_{CO_2} - \frac{P_{H_2}^{\ 2}P_{CO}^{\ 2}}{K_{ref}}\right)}{(1 + K_{CH_4}P_{CH_4} + K_{CO_2}P_{CO_2})^2}$	Ir/Al_2O_3	33
19	$r_{ref} = \frac{k_{ref}P_{CH_4}P_{CO_2}}{(1 + K_1P_{CH_4} + K_2P_{CO})(1 + K_3P_{CO_2})}$	$Ni/La/Al_2O_3$	36
20	$r_{ref} = \frac{k_{ref}\sqrt{K_1K_2P_{CH_4}P_{CO_2}}}{(1 + \sqrt{K_1P_{CH_4}} + \sqrt{K_2P_{CO_2}})^2}$	Ni/Al_2O_3, Ni/SiO_2, $Ni/CaO-Al_2O_3$	37
21	$r_{ref} = \frac{k_3K_1K_2P_{CH_4}P_{CO_2}P_{CO}P_{H_2}^{\ 2}}{(P_{CO}P_{H_2}^{\ 2} + K_1P_{CH_4}P_{CO} + K_2P_{CO_2}P_{H_2}^{\ 2})^2}$	Ni/SiO_2	38
22	$r_{ref} = \frac{k_1P_{CH_4}P_{CO_2}}{\left(\frac{k_{-1}K}{k_7}\right)P_{CO}P_{H_2}^{\ (4-x)/2} + \left[1 + \left(\frac{k_1}{k_7}\right)P_{CH_4}\right]P_{CO_2}}$	supported Pt and Ni	27, 28
23	$r_{ref} = \frac{k_{ref}P_{CH_4}P_{CO_2}}{(1 + K_{CH_4}P_{CH_4})(1 + K_{CO_2}P_{CO_2})}$	Ni/Al_2O_3, $Ni/CeO_2-Al_2O_3$	39

a commercial software package, InTouch by Wonderware. Most of the operating conditions can be set directly from the computer, with the exception being the reactor pressure, which has to be adjusted manually by using the back-pressure regulator. The computer logs in data automatically at operator-determined intervals. The unit is designed to operate up to a pressure of 100 psig and a temperature of 900 °C.

The unit has four lines for gas feeds, each being independently controlled by a Brooks mass flow controller. The reactor consists of a silica-lined stainless steel tube of a nominal outer diameter of 13 mm (0.5 in.) and a nominal length of 0.6 m (25 in.), placed in a 0.45-m (18-in.) single-zone furnace from Applied Test Systems. A passivating lining of silica on the stainless steel reactor tube was applied at Restek Corp. The catalyst is placed in the center of the reactor, with quartz chips placed upstream and downstream of the catalyst. The product stream is sampled immediately downstream using a six-port external-volume gas-sampling valve manufactured by Valco Instruments Co. Inc. The valve is set at the operating pressure of the reactor and a minimum temperature of 100 °C. Between the reactor outlet and the sampling valve, the hot gases are cooled, to prevent them from heating the valve to a temperature beyond its operating range. The exit gas stream from the sampling loop is passed through a back-pressure regulator with an operating range of 0−2000 psig. This

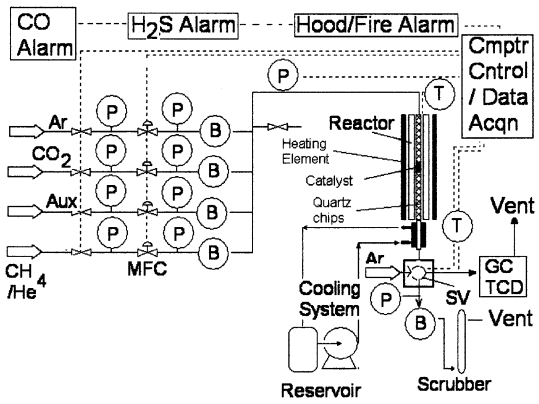

Figure 1. Flowsheet of the catalyst testing unit: B, back-pressure regulator; GC TCD, gas chromatograph with a thermal conductivity detector; MFC, mass flow controllers; P, pressure gauge; SV, sample valve; T, thermocouple.

back-pressure regulator is used to maintain the reactor pressure. The pressure in the reactor is monitored by a Sensotec pressure transducer with an operating range of 0−2000 psig.

The products are analyzed online by a Hewlett-Packard (HP) 5890 gas chromatograph (GC) using two columns and two detectors in parallel. The GC is controlled using HP Chemstation software by the same computer in a multitasking MS Windows environment. In the GC, the flow is split between the two columns: a HayeSep-DB packed column, 9 m × 3.1 mm (30 ft × $^1/_8$ in.), and a J&W DBWax capillary column, 20 m × 0.1 mm i.d. The oven temperature for both of the columns is maintained isothermally at 150 °C. The packed column is connected to a thermal conductivity detector (TCD), which provides quantitative analysis for He, H_2, CO, CH_4, CO_2, and H_2O. Helium is used as the internal standard while argon serves as the carrier gas. All of the gas mixtures were obtained from Airgas. The capillary column is connected to a flame ionization detector (FID) used to detect whether any other products such as oxygenates are being produced in the reaction. The GC feed line from the sampling loop is maintained at a temperature of 150 °C by wrapping the line with heating tape. The tubing between the exit of the reactor and the inlet of the sample loop is maintained at 150 °C similarly. These modifications prevent the water in the product stream from condensing before reaching the GC inlet and the sampling loop, respectively.

The entire unit is located in a walk-in hood. The computer continuously monitors alarms for CO and for flows of reactive gases, hood velocity, ambient hood temperature, reactor temperature, reactor pressure, and electric power. The unit automatically shuts down in the event of hood failure, fire, power and air supply failure, or CO leak detection or if the gas flows or reactor temperature exceeds preset operating ranges.

Catalyst Pretreatment. The unsupported cobalt−tungsten η-carbide (Co_6W_6C) to be used as a precursor for methane dry reforming catalyst was obtained from Nanodyne Inc. and had an initial nitrogen Brunauer−Emmett−Teller surface area of 5 m^2/g. Typically, 0.3 g of the material with a particle size of less than 38 μm was used in each run. A three-step in situ pretreatment procedure was developed to obtain an active and stable catalyst from the precursor. Argon was used as an inert, and He was the internal standard for all of the calculations.

Table 2. Experimental Design for the Kinetic Study of the CO_2 Reforming of CH_4 with Co_6W_6C Catalyst (Particle Size < 38 μM, Weight of Catalyst Used = 0.3 g, Total Feed WHSV = 11 200 scc/h/g of Catalyst, P_{Total} = 5 atm)

		partial pressure (atm.)			
label	T (°C)	CH_4	CO_2	Ar	sequence
AA	600	1	0.5	3.5	1
AB	600	1	1	3	2, 7
AC	600	1	2	2	3
AD	600	1	3	1	4
AE	600	1	4	0	5
AF	600	0.5	1	3.5	6
AG	600	2	1	2	8
AH	600	3	1	1	9
AI	600	4	1	0	10
BA	550	1	0.5	3.5	11
BB	550	1	1	3	12, 17
BC	550	1	2	2	13
BD	550	1	3	1	14
BE	550	1	4	0	15
BF	550	0.5	1	3.5	16
BG	550	2	1	2	18
BH	550	3	1	1	19
BI	550	4	1	0	20
CA	500	1	0.5	3.5	21
CB	500	1	1	3	22, 27
CC	500	1	2	2	23
CD	500	1	3	1	24
CE	500	1	4	0	25
CF	500	0.5	1	3.5	26
CG	500	2	1	2	28
CH	500	3	1	1	29
CI	500	4	1	0	30

In the first step, the Co_6W_6C material was heated in situ by flowing H_2 (62 sccm) at 400 °C and atmospheric pressure for 1 h. Subsequently, the system was flushed with Ar (190 sccm) at 400 °C and atmospheric pressure for 1 h. In the third step, the feed mixture was introduced into the system (at a weight hourly space velocity, WHSV, of 11 200 scc/h/g of catalyst) with the feed ratio maintained at $CH_4/CO_2/Ar = 1/1/3$ and under a total pressure of 5 atm. The reaction temperature was raised from 400 to 850 °C over 1.5 h and was then maintained at 850 °C in the flowing reactant mixture. The catalyst activity first increases with time at 850 °C and then levels off within a time span of about 24 h, staying at that level for over 150 h.[14,40] Hence, the catalyst was first stabilized at 850 °C for about 50 h, and the kinetic experiments were subsequently carried out.

Experimental Design. The independent variables considered for the kinetic study are the reaction temperature and the partial pressures of methane, carbon dioxide, and inert (Ar), obtained from the inlet feed stream. The dependent variables comprise the partial pressures of hydrogen, carbon monoxide, and water, obtained from the product stream. The experiments were performed under differential reaction conditions (i.e., total reactant conversions of approximately 10% or less) over a temperature range of 500−600 °C. The total WHSV of the feed mixture was maintained at 11 200 scc/h/g of catalyst. The total operating pressure was fixed at 5 atm. The partial pressure of each of the two reactants (CH_4 and CO_2) was varied from 0.5 to 4 atm, retaining the partial pressure of the other reactant at 1 atm. The details of the experiments performed in this study are listed in Table 2.

The reaction temperature was first held constant at 600 °C for approximately 2 h before starting any run at

that specific temperature. Each run was then carried out for 2 h. After all of the data was collected at that temperature, the catalyst activity was subsequently checked for any possible deactivation at 850 °C with a feed ratio of $CH_4/CO_2/Ar = 1/1/3$. However, no significant change in the catalyst activity was ever observed for repeated runs at 850 °C. Hence, the possibility of catalyst deactivation during the runs was ruled out. After performance of the set of experiments at 600 °C (and checking for deactivation at 850 °C), the reaction temperature was then lowered to 550 °C and then subsequently to 500 °C, and the above procedure was repeated at every temperature. The product samples downstream of the reactor were analyzed online at 15-min intervals. The reactor reaches steady state after 30−45 min. The data were obtained from the samples collected after the first hour of the run.

Results and Discussion

Effect of the Partial Pressure of the Reactants. In this study, the experimental data for the rates of product formation were found to be more reliable and sensitive to small conversions for the differential operating conditions, as compared to the rates of consumption of the reactants. Hence, the entire focus is directed toward the modeling of the rates of production of CO, H_2, and H_2O.

As mentioned earlier, all of the experiments of Table 2 were performed under differential reaction conditions, with total reactant conversions of approximately 10% or less. The major reaction products consisted of carbon monoxide, hydrogen, and water. The overall carbon balances obtained for these experiments were 101−103%. The details of the calculation for the partial pressures and the rates of formation are given elsewhere.[40]

Figures 2−4 show the observed rates of formation for each of the product species, H_2, CO, and H_2O, at 600, 550, and 500 °C, respectively. The rate of formation of CO is always higher than that of H_2 and H_2O combined, at all reaction conditions. Besides, the rate of formation of H_2 becomes less than that of H_2O for decreasing reaction temperatures. These figures clearly show an increase in the magnitude of the rates for increasing temperatures. The rates of CO and H_2O formation depend on the partial pressure of CO_2 to a greater extent than they depend on that of CH_4. On the other hand, the rate of H_2 formation is governed mostly by the partial pressure of CH_4.

Comparison with Other Catalysts. Comparison with other results in the literature is difficult because conditions are seldom identical and often unspecified. However, in a few cases, comparisons are possible between the present catalyst, other unsupported carbides,[42] and supported nickel catalysts.[31,43] These comparisons, summarized in Table 3, are for the consumption of methane per unit time, per unit surface area (of the metal, if supported). To allow for concentration effects, the rates are divided by the partial pressures of CH_4 and CO_2. Especially for the supported nickel catalysts, which are prone to deactivation, the values of the rates are for short times on stream.

The results indicate that the bimetallic carbide catalyst has a higher specific activity than the other catalysts, especially at the higher temperatures.

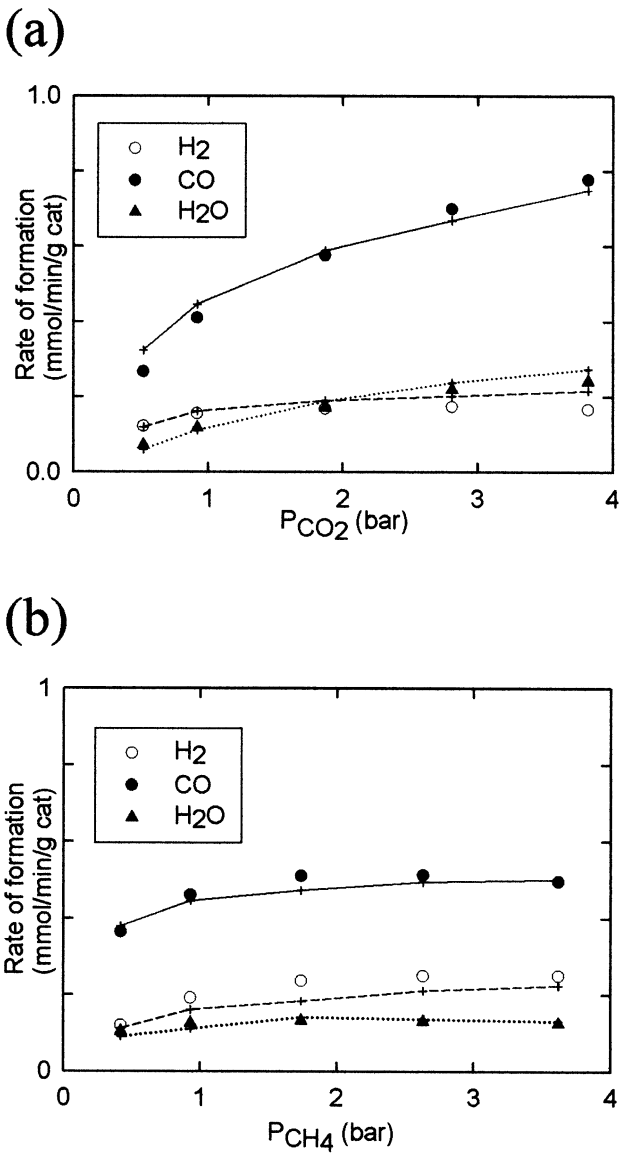

Figure 2. Effect of the reactant partial pressures on the rates of formation of different reaction species for the CO_2 reforming of CH_4 with Co_6W_6C catalyst (T = 600 °C, particle size < 38 μm, total feed WHSV = 12 100 scc/h/g of catalyst, and P_{total} = 5 atm). Lines denote the LH model. (a) Effect of P_{CO_2} (P_{CH_4} = 1 bar). (b) Effect of P_{CH_4} (P_{CO_2} = 1 bar).

Power-Law Model. A simple power-law model (eq 5) was first used to describe the rates of formation of each of the products H_2, CO, and H_2O. The reaction rate constant, k, was further expressed in the Arrhenius form. The values of these parameters are tabulated in Table 4, along with the coefficient of determination (R^2) obtained for the entire set of experiments. Comparisons of the observed (experimental) rates of formation of each of the species with those predicted by the power-law model are given in Figures 5−7. The data set includes all of the experiments given in Table 2. The model fits the observed data quite well. Further, the apparent activation energy (E_a) obtained for each of the species H_2, CO, and H_2O is comparable to those obtained earlier[40] from the initial catalyst activity over a wider temperature range, 500−850 °C.

Reaction Schemes and Thermodynamic Analysis. We have seen earlier that the entire methane-reforming reaction system consists of a complex network of parallel reactions. However, not all of the reactions

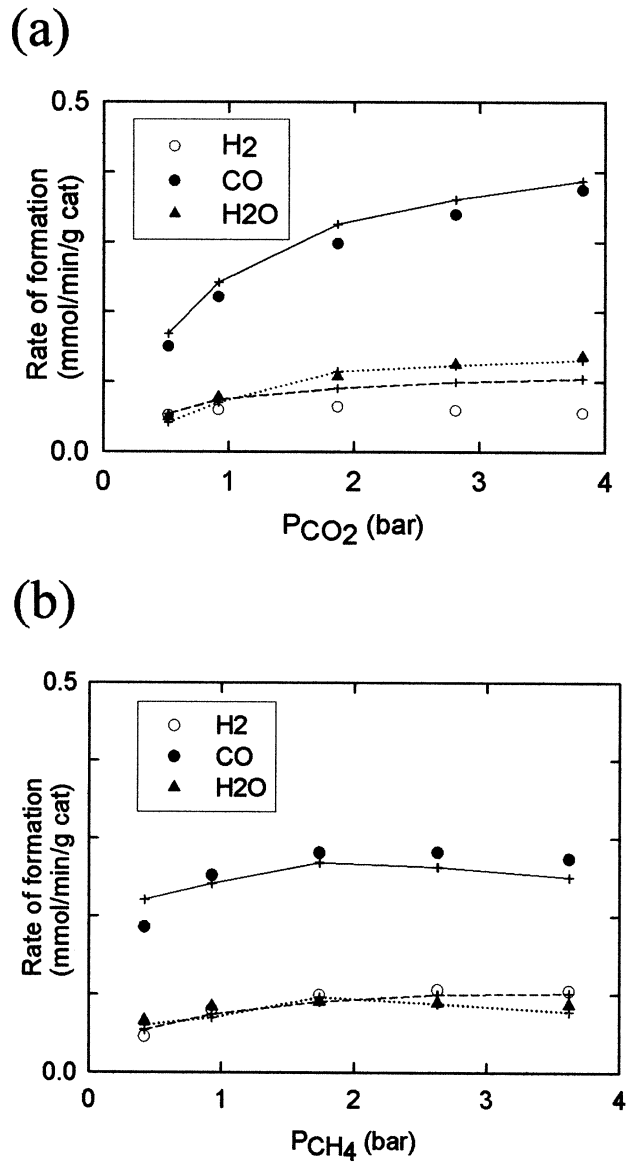

Figure 3. Effect of the reactant partial pressures on the rates of formation of different reaction species for the CO_2 reforming of CH_4 with Co_6W_6C catalyst (T = 550 °C, particle size < 38 μm, total feed WHSV = 11 200 scc/h/g of catalyst, and P_{total} = 5 atm). Lines denote the LH model. (a) Effect of P_{CO_2} (P_{CH_4} = 1 bar). (b) Effect of P_{CH_4} (P_{CO_2} = 1 bar).

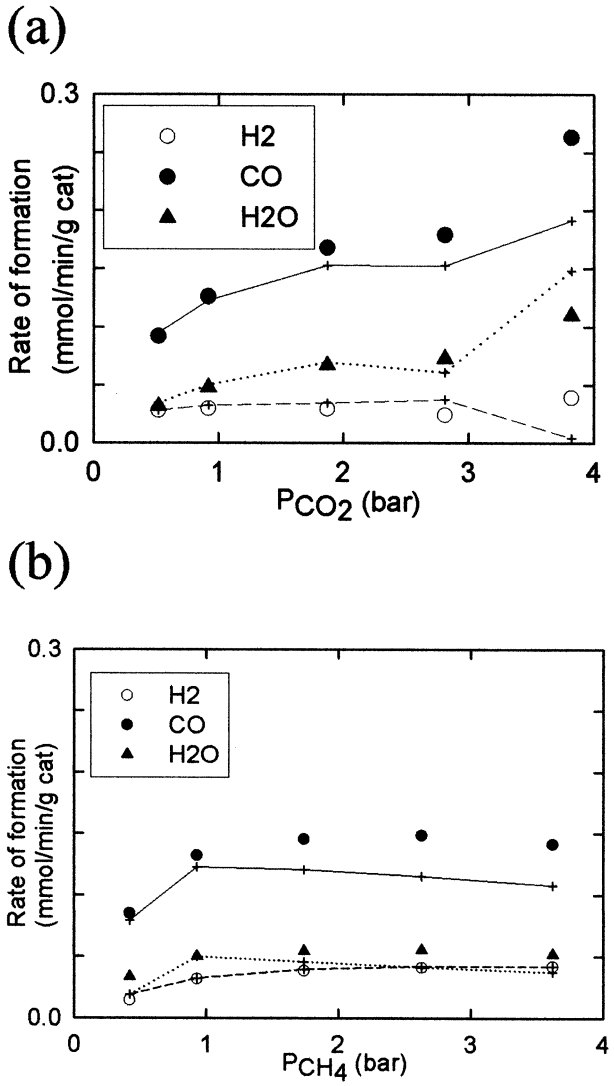

Figure 4. Effect of the reactant partial pressures on the rates of formation of different reaction species for the CO_2 reforming of CH_4 with Co_6W_6C catalyst (T = 500 °C, particle size < 38 μm, total feed WHSV = 11 200 scc/h/g of catalyst, and P_{total} = 5 atm). Lines denote the LH model. (a) Effect of P_{CO_2} (P_{CH_4} = 1 bar). (b) Effect of P_{CH_4} (P_{CO_2} = 1 bar).

from this complex set of parallel reactions are required to depict the whole reaction network. Only a few stoichiometrically independent reactions would suffice to describe the reaction system. The reaction scheme considered in our study consists of eq 10a,b,e and the reverse of eq 10f; these are repeated below for the sake of clarity:

$$CH_4 + CO_2 \rightarrow 2CO + 2H_2 \quad \text{(MR)} \quad (24a)$$

$$CO_2 + H_2 \rightleftarrows H_2O + CO \quad \text{(RWGS)} \quad (24b)$$

$$CH_4 \rightarrow 2H_2 + C \quad \text{(CD)} \quad (24c)$$

$$CO_2 + C \rightarrow 2CO \quad \text{(RB)} \quad (24d)$$

For each of the reactions in eq 24, for temperatures in the range of 500−850 °C, the values of the equilibrium constant K_a were calculated and compared with the values of the appropriate ratios of the partial pressures of the vapor-phase components. The equilibrium constant, K_a, for every reaction was obtained as a function of temperature from the software CHEMEQ.BAS developed by Sandler.[44] The details of the calculations are given elsewhere[40] and are computed as per the procedure outlined by Sandler.[44] For the MR reaction (eq 24a), the value of the ratio of the observed partial pressures is found to be considerably less (by 3−4 orders of magnitude) than the calculated value of the thermodynamic equilibrium constant (K_a) for all of the experimental runs. Hence, the overall MR reaction was assumed to be (practically) irreversible. However, the RWGS reaction (eq 24b) was assumed to be reversible but not in equilibrium, based on a similar analysis of the partial pressure ratios.[40] This is contrary to the usual assumption for the RWGS reaction, which is generally taken to be in equilibrium when the reaction is carried out over other catalysts.[7,27,38]

LH Model. On the basis of the various possible reaction mechanisms and adsorption-based kinetic models described earlier, we used the following simple reaction mechanism:

Table 3. Comparison of Specific Activity with Those of Other Catalysts

	pseudo-second-order rate constant for loss of methane[a] (μmol/s/m^2/atm^2)						
catalyst	T = 600 °C	T = 650 °C	T = 700 °C	T = 750 °C	T = 800 °C	T = 850 °C	ref
Co_6W_6C (unsup)	0.47	1.25	1.79	2.67	3.72	4.31	this work[b]
Ni/C	0.39	0.23	0.12	0.24	0.26		31[c]
Ni/C−HCl	0.18	0.16	0.19	0.21	0.32		
Ni/C−HNO_3	0.098	0.098	0.11	0.14	0.19		
Ni/C−HF	0.094	0.094	0.10	0.14	0.23		
Mo_2C(I) (unsup)						1.4	42[d]
Mo_2C(II) (unsup)						0.89	

[a] Average rate of loss of methane per unit surface area (of metal component, if supported) divided by the inlet partial pressure of methane and the inlet partial pressure of carbon dioxide. All data shown were obtained when the inlet partial pressures are equal. [b] $P_{CH_4,in} = 1$ atm $= P_{CO_2,in}$. [c] $P_{CH_4,in} = 1.6$ atm $= P_{CO_2,in}$, estimated from data in work by Wang and Lu.[43] [d] $P_{CH_4,in} = 0.5$ atm $= P_{CO_2,in}$, estimated from "ambient" total pressure.

Table 4. Parameter Estimates of the Power-Law Model

reaction species	preexponential factor, k_0 (mol/min/g of catalyst/atm^{m+n})	apparent activation energy, E_a (kcal/mol)	m	n	R^2
H_2	509.2	25.86	0.39	0.06	0.97
CO	21.67	18.6	0.17	0.43	0.98
H_2O	0.3981	13.86	0.11	0.50	0.97

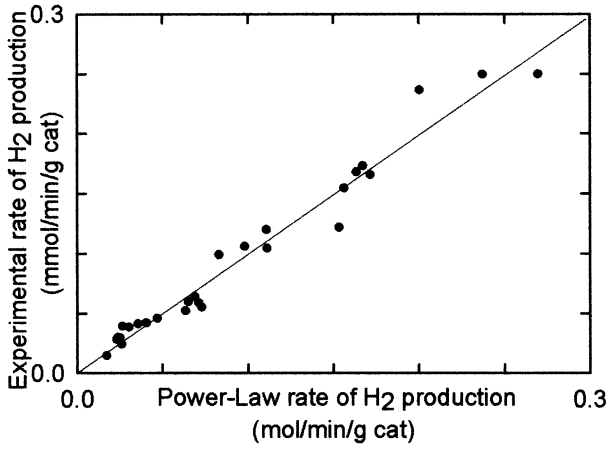

Figure 5. Comparison plot for the net rates of H_2 formation by the power-law model.

$$CH_4 + * \overset{K_1}{\rightleftharpoons} CH_x* + [(4 - x)/2]H_2 \quad (25a)$$

$$CO_2 + * \overset{K_2}{\rightleftharpoons} CO + O* \quad (25b)$$

$$CH_x* + O* \overset{k_3}{\longrightarrow} CO + (x/2)H_2 + 2* \quad (25c)$$

$$CH_x* \overset{K_4}{\rightleftharpoons} C* + (x/2)H_2 \quad (25d)$$

$$H_2 + O* \underset{k_{-5}}{\overset{k_5}{\rightleftharpoons}} H_2O + * \quad (25e)$$

$$C* + O* \overset{k_6}{\longrightarrow} CO + 2* \quad (25f)$$

The parameter x is assumed to equal a value of 2 for the sake of simplicity. Further, most of these steps can be expressed as a series of simpler steps to yield a more comprehensive mechanism. However, this would increase the number of parameters involved. To simplify the mathematical modeling, the detailed steps are not considered in this reaction sequence.

The first and second steps are assumed to be in equilibrium. The third step, eq 25c, is slow and irreversible. The next step, eq 25d, is assumed to be in equilibrium because the net rate of carbon formation is small compared to the rate of formation of other products. This was confirmed[40] from the carbon balances for the system at different temperatures. The reaction between adsorbed oxygen and gaseous H_2 to produce water in eq 25e is assumed to be reversible, but not in equilibrium, because the RWGS reaction was assumed to be not in equilibrium, previously. The final step, eq 25f, signifies the removal of accumulated carbon from the reaction system as described earlier. This is observed in the experimental data. The reaction scheme of eq 24, comprising the four reactions MR, RWGS, CD, and RB, can be expressed as a simple combination of the various steps of the reaction mechanism proposed previously. For example, RB can be expressed as a combination of eqs 25b and 25f. RB is irreversible

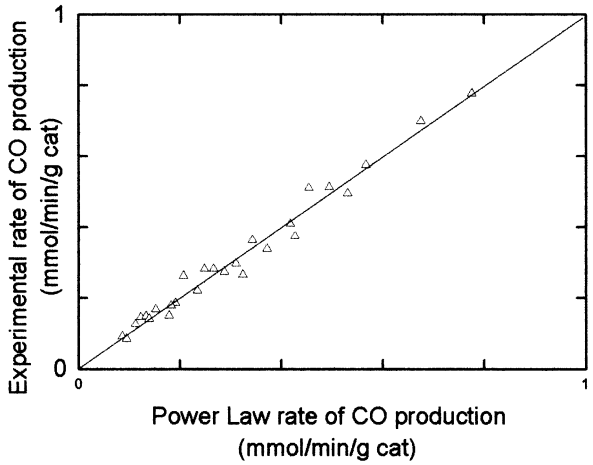

Figure 6. Comparison plot for the net rates of CO formation by the power-law model.

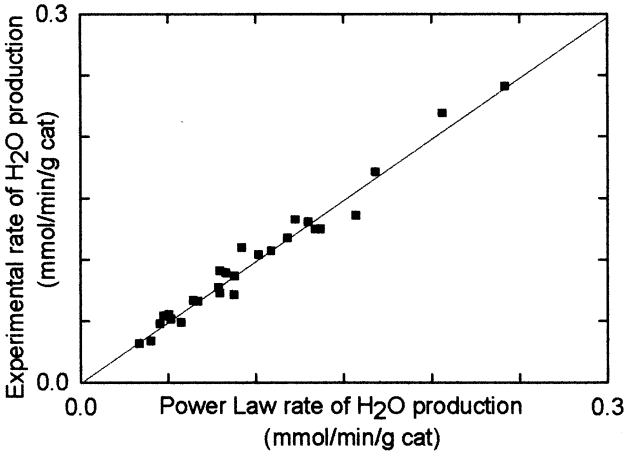

Figure 7. Comparison plot for the net rates of H_2O formation by the power-law model.

because eq 25f is irreversible. In particular, CD can be shown to be a combination of eqs 25a and 25d. Because eq 25a is in equilibrium and eq 25d is (approximately) in equilibrium, CD is (approximately) in equilibrium. This would seem to be in contradiction to the thermodynamic calculation alluded to earlier, but the approximation is justified beause of the very low rate of CD, as noted earlier.

From the above reaction mechanism, the expressions for the rate of formation of the products can be written as

$$r_{CO} = k_3\theta_{CH_2}\theta_O + k_6\theta_C\theta_O \tag{26a}$$

$$r_{H_2} = k_3\theta_{CH_2}\theta_O + k_{-5}P_{H_2O}\theta_S - k_5P_{H_2}\theta_O \tag{26b}$$

and

$$r_{H_2O} = k_5P_{H_2}\theta_O - k_{-5}P_{H_2O}\theta_S \tag{26c}$$

Here θ_I is the fraction of the active sites covered by species I for $I = CH_2$, C, and O, and θ_S is the fraction of free active sites. These are related through a balance on all sites

$$\theta_{CH_2} + \theta_C + \theta_O + \theta_S = 1 \tag{26d}$$

and through the equilibrium relationships

$$K_1 = \frac{\theta_{CH_2}P_{H_2}}{\theta_S P_{CH_4}} \tag{27a}$$

$$K_2 = \frac{\theta_O P_{CO}}{\theta_S P_{CO_2}} \tag{27b}$$

and

$$K_4 \approx \frac{\theta_C P_{H_2}}{\theta_{CH_2}} \tag{27c}$$

From eqs 26 and 27, the rates of formation of the products can be obtained in terms of rate constants, equilibrium constants, and partial pressures as

$$r_{CO} = \frac{K_1K_2}{den^2}\left(\frac{P_{CH_4}P_{CO_2}}{P_{CO}P_{H_2}}\right)\left(k_3 + \frac{k_6K_4}{P_{H_2}}\right) \tag{28a}$$

$$r_{H_2} = \frac{k_3K_1K_2}{den^2}\left(\frac{P_{CH_4}P_{CO_2}}{P_{CO}P_{H_2}}\right) - \frac{k_5K_2}{den}\left(\frac{P_{H_2}P_{CO_2}}{P_{CO}}\right) + \frac{k_{-5}P_{H_2O}}{den} \tag{28b}$$

$$r_{H_2O} = \frac{k_5K_2}{den}\left(\frac{P_{H_2}P_{CO_2}}{P_{CO}}\right) - \frac{k_{-5}P_{H_2O}}{den} \tag{28c}$$

where

$$den = 1 + K_1\left(\frac{P_{CH_4}}{P_{H_2}}\right) + K_2\left(\frac{P_{CO_2}}{P_{CO}}\right) + K_1K_4\left(\frac{P_{CH_4}}{P_{H_2}^2}\right) \tag{28d}$$

Parameter Estimation for the LH Model. Values of the reaction rate constants k_3, k_6, k_5, and k_{-5} and the apparent adsorption equilibrium constants K_1, K_2, and K_4 were estimated using nonlinear least-squares analysis and the Marquardt−Levenberg algorithm. Estimation of the parameters was based on the minimization of the sum of residual squares of the observed experimental reaction rates and the predicted rates for each species obtained from eq 28.

The initial step consisted of determining the parameters from each of eq 28a−d at the highest temperature. Equation 28a was first solved for the parameters k_3, k_6, K_1, K_2, and K_4 at 600 °C. Using these values in eq 28b, the values of the remaining constants k_5 and k_{-5} at 600 °C were obtained. Then the values of all seven parameters were used as the initial guess in eq 28c; the solution converged, but to a slightly different set of values. These new values now served as the initial guess, and the procedure was again repeated for the three relations, eqs 28a−c, in turn. After a few cycles, the values of the parameters were used as the initial guess for the simultaneous solution of all three relations, still at 600 °C.

Now the entire procedure was repeated for obtaining the values of the parameters at 550 °C and subsequently at 500 °C. The values of the parameters obtained at 600 °C were used as the starting initial guess for the estimation at 550 °C, and similarly the values estimated at 550 °C were used for the parameter estimation at 500 °C.

After the values of all of the parameters were obtained at 500, 550, and 600 °C, the parameters were related at all temperatures by the Arrhenius and van't Hoff equations

$$k_i = a_i \exp(-E_i/RT) \tag{29a}$$

$$K_i = A_i \exp(-\Delta H_i/RT) \tag{29b}$$

where a_i and A_i are preexponential factors for rate constants k_i and apparent adsorption equilibrium constants K_i, respectively, E_i is an apparent activation energy, and ΔH_i is an apparent adsorption enthalpy. Estimates of the values of a_i, A_i, E_i, and ΔH_i were obtained by best-fitting the values of k_i and K_i obtained earlier at the three temperatures.

These values now served as the initial guess for the final iterations using all of the observed experimental data, the three nonlinear relations (eq 28) and the temperature dependence of the rate constants and the adsorption coefficients (eq 29). Thus, a set of 81 data points (the rates of formation of H_2, CO, and H_2O for all of the partial pressures at all of the reaction temperatures) was considered for the final estimation of 14 parameters.

The parameters were successfully estimated and are tabulated in Table 5. Also shown in Table 5 are the values of the rate constants and the apparent adsorption equilibrium constants at the middle temperature, 550 °C. Finally, the coefficient of determination (R^2) of the final estimated parameters equals 0.98. This is comparable to the values of R^2 in Table 4 for the power-law model.

It should be noted that the values of the apparent adsorption enthalpies ΔH_i in Table 5 do not satisfy all of the thermodynamic rules for adsorption enthalpy.[45,46] This can be attributed to the fact that each step of eq 25a−f actually consists of a number of detailed sequential steps that are lumped together for ease of mathematical modeling, as seen earlier. Each ΔH_i in Table 5 includes the adsorption enthalpy of at least one surface-reaction step, which could be either endothermic

Table 5. Parameter Estimates for the LH Model

parameter	estimate	unit
A_1	3.4×10^{-6}	
ΔH_1	−2.46	kcal/mol
K_1(550 °C)	1.5×10^{-5}	
A_2	1.32×10^{-2}	
ΔH_2	−3.31	kcal/mol
K_2(550 °C)	0.10	
a_3	1.51×10^{11}	mol/min/g of catalyst
E_3	38.0	kcal/mol
k_3(550 °C)	12.2	mol/min/g of catalyst
A_4	1.03×10^{11}	atm
ΔH_4	32.3	kcal/mol
K_4(550 °C)	273	atm.
a_5	0.26	mol/min/atm/g of catalyst
E_5	4.58	kcal/mol
k_5(550 °C)	1.6×10^{-2}	mol/min/atm/g of catalyst
a_{-5}	8.06×10^{4}	mol/min/atm/g of catalyst
E_{-5}	29.6	kcal/mol
K_{-5} (550 °C)	1.1×10^{-3}	mol/min/atm/g of catalyst
a_6	1.09×10^{5}	mol/min/g of catalyst
E_6	30.2	kcal/mol
k_6(550 °C)	1.0×10^{-3}	mol/min/g of catalyst

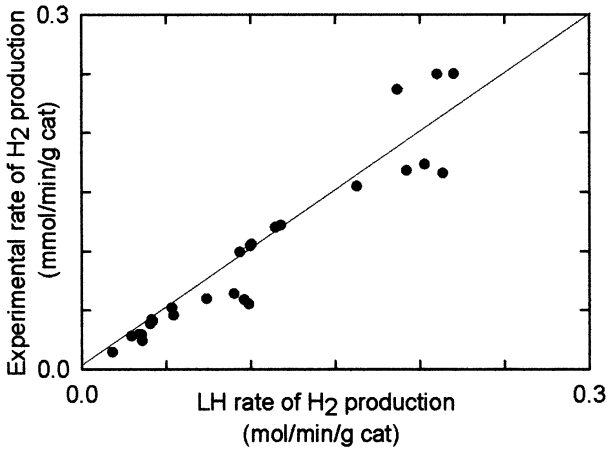

Figure 8. Comparison plot for the net rates of H_2 formation by the LH model.

or exothermic. Hence, ΔH_i represents an apparent adsorption enthalpy and not the true adsorption enthalpy.

Using the values of Table 5, we have calculated reaction rates predicted by the model as a function of increasing reactant partial pressure for the various temperatures used experimentally. These points are shown in Figures 2−4 by +'s and are connected by straight lines, so that the predictions can be compared with the observed values.

Figures 8−10 represent comparison plots for formation rates for all of the product species. In all cases, the model gives a reasonably good fit to the observed experimental data. Side-by-side visual comparisons of component reaction-rate predictions by the power-law model (Figures 5−7) with Figures 8−10 might seem to indicate a better fit by the power-law model, at least for H_2 and H_2O, but this is contrary to the fact that the values of R^2 for the two models are comparable. Note, however, that the power-law model has only 12 adjustable parameters while the LH model contains 14 adjustable parameters.

Conclusions

The kinetics of CO_2 reforming of methane with a catalyst obtained from the Co_6W_6C precursor was studied under differential conditions over a temperature range of 500−600 °C, based on a detailed experimental design. The rates of formation of the products H_2, CO, and H_2O were used for the kinetic analysis. The observed rates follow a LH type of reaction mechanism. The rate of CO production was always greater than the combined rates of H_2 and H_2O production for all reaction conditions. This could be attributed to the carbon removal by the RB reaction. The carbon accumulation in the system occurs during the third stage of the catalyst pretreatment procedure. A simple reaction scheme consisting of four reactions was considered, and the thermodynamic analysis showed that the reactions were not in equilibrium.

A simple power-law model was first used for effectively describing the kinetics for each of the product species H_2, CO, and H_2O. However, the model is incapable of incorporating all of the mechanistic details involved in the reaction system. Hence, a LH type of kinetic model was proposed based on a simplified reaction mechanism. The mechanism incorporates CD as well as carbon removal occurring in the reaction system, both of which are generally disregarded in most of the reported kinetic models. The parameters of the model were successfully estimated for all of the experimental data. The comparison plots of the observed data and the predicted models (power-law and LH) show generally a good fit for all of the product species.

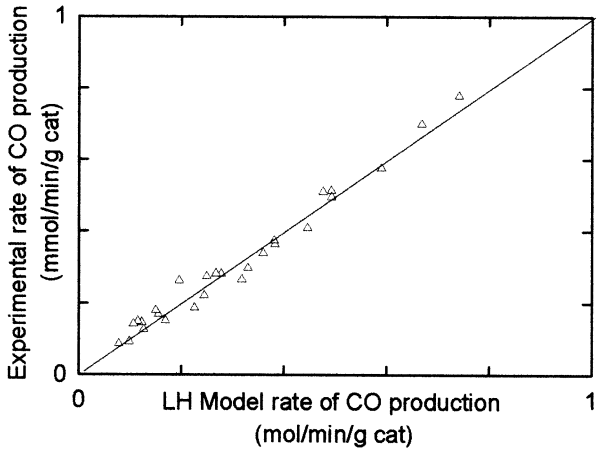

Figure 9. Comparison plot for the net rates of CO formation by the LH model.

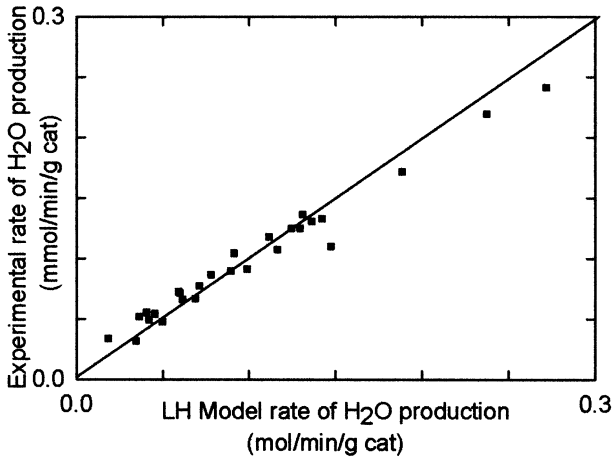

Figure 10. Comparison plot for the net rates of H_2O formation by the LH model.

Acknowledgment

Financial support from U.S. Department of Energy under Cooperative Agreement DE-AC22-99FT40540 with the Consortium of Fossil Fuel Science is gratefully acknowledged. We thank J.B. Cropley for his useful suggestions during this study.

Literature Cited

(1) Otsuka, K.; Ushiyama, T.; Yamanaka, I. Partial Oxidation of Methane by Redox Reaction with Cerium Oxide. *Chem. Lett.* **1993**, *9*, 1517.

(2) Seshan, K.; tan Barge, H. W.; Hally, W.; van Keulen, A. N. J.; Ross, J. R. H. Carbon Dioxide Reforming of Methane in the Presence of Nickel and Platinum Catalysts Supported on ZrO_2. *Stud. Surf. Sci. Catal.* **1994**, *81*, 285.

(3) Ross, J. R. H.; van Keulen, A. N. J.; Hegarty, M. E. S.; Seshan, K. The Catalytic Conversion of Natural Gas to Useful Products. *Catal. Today* **1996**, *30*, 193.

(4) Wang, S.; Lu, G. Q.; Millar, G. J. Carbon Dioxide Reforming of Methane to Produce Synthesis Gas over Metal-Supported Catalysts: State of the Art. *Energy Fuels* **1996**, *10*, 896.

(5) Claridge, J. B.; York, A. P. E.; Brungs, A. J.; Marquez-Alvarez, C.; Sloan, J.; Tsang, S. C.; Green, M. L. H. New Catalysts for the Conversion of Methane to Synthesis Gas: Molybdenum and Tungsten Carbide. *J. Catal.* **1998**, *180*, 85.

(6) Rostrup-Neilson, J. R.; Bak-Hansen, J. H. CO_2-Reforming of Methane over Transition Metals *J. Catal.* **1993**, *144*, 38.

(7) Bradford, M. C. J.; Vannice, M. A. CO_2 Reforming of CH_4. *Catal. Rev. Sci. Eng.* **1999**, *41* (1), 1.

(8) Rostrup-Neilsen, J. R. Syngas in Perspective. *Catal. Today* **2002**, *71*, 243.

(9) York, A. P. E. Magic Catalysts. *Chem. Br.* **1999**, *35* (8), 25.

(10) Brungs, A. J.; York, A. P. E.; Green, M. L. H. Comparison of the Group V and VI Transition Metal Carbides for Methane Dry Reforming and Thermodynamic Prediction of their Relative Stabilities. *Catal. Lett.* **1999**, *57*, 65.

(11) Brungs, A. J.; York, A. P. E.; Claridge, J. B.; Marquez-Alvarez, C.; Green, M. L. H. Dry Reforming of Methane to Synthesis Gas over Supported Molybdenum Carbide Catalysts. *Catal. Lett.* **2000**, *70*, 117.

(12) Oshikawa, K.; Nagai, M.; Omi, S. Active Species of Molybdenum Carbide Catalysts in Methane Reforming: η-Mo_3C_2. *Chem. Lett.* **2000**, *9*, 1086.

(13) Shamsi, A.; Lyons, D. Methane Dry Reforming over Carbide, Ni-Based, and Noble Metal Catalysts. *Prepr.—Am. Chem. Soc., Div. Pet. Chem.* **2000**, *45* (1), 132.

(14) Iyer, M. V.; Norcio, L. P.; Punnoose, A.; Kugler, E. L.; Seehra, M. S.; Dadyburjor, D. B. Catalysis for Synthesis Gas Formation from Reforming of Methane. *Top. Catal.* **2003**, submitted for publication.

(15) Sakai, Y.; Saito, H.; Sodesawa, T.; Nozaki, F. Catalytic Reactions of Hydrocarbon with Carbon Dioxide over Metallic Catalysts. *React. Kinet. Catal. Lett.* **1984**, *24*, 253.

(16) Tokunaga, O.; Ogasawara, S. Reduction of Carbon Dioxide with Methane over Ni-Catalyst. *React. Kinet. Catal. Lett.* **1989**, *39* (1), 69.

(17) Richardson, J. T.; Paripatyadar, S. A. Carbon Dioxide Reforming of Methane with Supported Rhodium. *Appl. Catal.* **1990**, *61* (2), 293.

(18) Erdohelyi, A.; Cserenyi, J.; Papp, E.; Solymosi, F. Catalytic Reaction of Methane with Carbon Dioxide over Supported Palladium. *Appl. Catal. A* **1994**, *108* (2), 205.

(19) Takano, A.; Tagawa, T.; Goto, S. Carbon Dioxide Reforming of Methane on Supported Nickel Catalysts. *J. Chem Eng. Jpn.* **1994**, *27* (6), 727.

(20) Bodrov, I. M.; Apel'baum, L. O. Reaction Kinetics of Methane and Carbon Dioxide on a Nickel Surface. *Kinet. Catal.* **1967**, *8* (2), 379.

(21) Erdohelyi, A.; Cserenyi, J.; Solymosi, F. Activation of CH_4 and its Reaction with CO_2 over supported Rh Catalysts. *J. Catal.* **1993**, *141*, 287.

(22) Nakamura, J.; Aikawa, K.; Sato, K.; Uchijima, T. Role of Support in Reforming of CH_4 with CO_2 over Rh Catalysts. *Catal. Lett.* **1994**, *25*, 265.

(23) Osaki, T.; Horiuchi, T.; Suzuki, K.; Mori, T. Suppression of Carbon Deposition in CO_2 Reforming of Methane on Metal Sulfide Catalysts. *Catal. Lett.* **1995**, *35*, 39.

(24) Efstathiou, A. M.; Kladi, A.; Tsipouriari, V. A.; Verykios, X. E. Reforming of Methane with Carbon Dioxide to Synthesis Gas over Supported Rhodium Catalysts. *J. Catal.* **1996**, *158*, 64.

(25) Mark, M. F.; Maier, W. F. CO_2-Reforming of Methane on Supported Rh and Ir Catalysts. *J. Catal.* **1996**, *164*, 122.

(26) Kroll, V. C. H.; Swaan, H. M.; Lacombe, S.; Mirodatos, C. Methane Reforming Reaction with Carbon Dioxide over Ni/SiO2 Catalyst. II. A Mechanistic Study. *J. Catal.* **1997**, *164*, 387.

(27) Bradford, M. C. J.; Vannice, M. A. CO_2 Reforming of CH_4 over supported Pt Catalysts. *J. Catal.* **1998**, *173*, 157.

(28) Bradford, M. C. J.; Vannice, M. A. Catalytic Reforming of Methane with Carbon Dioxide over Nickel Catalysts. II. Reaction Kinetics. *Appl. Catal. A* **1996**, *142*, 97.

(29) Osaki, T.; Fukaya, H.; Horiuchi, T.; Suzuki, K.; Mori, T. Isotope Effect and Rate-Determining Step of the CO_2-Reforming of Methane over Supported Ni Catalyst. *J. Catal.* **1998**, *180*, 106.

(30) Ferreira-Aparicio, P.; Marquez-Alvarez, C.; Rodriguez-Ramos, I.; Schuurman, Y.; Guerrero-Ruiz, A.; Mirodatos, C. A Transient Kinetic Study of the Carbon Dioxide Reforming of Methane over Supported Ru Catalysts. *J. Catal.* **1999**, *184*, 202.

(31) Lu, G. Q.; Wang, S. Ni-based Catalysts for Carbon Dioxide Reforming of Methane. *CHEMTECH* **1999**, *29* (1), 37.

(32) Luo, J. Z.; Yu, Z. L.; Ng, C. F.; Au, C. T. CO_2/CH_4 Reforming over $Ni-La_2O_3/5A$: An Investigation on Carbon Deposition and Reaction Steps. *J. Catal.* **2000**, *194*, 198.

(33) Mark, M. F.; Mark, F.; Maier, W. F. Reaction Kinetics of the CO_2 Reforming of Methane. *Chem. Eng. Technol.* **1997**, *20*, 361.

(34) Lewis, W. K.; Gilliland, E. R.; Reed, W. A. Reaction of Methane with Copper Oxide in a Fluidized Bed. *Ind. Eng. Chem.* **1949**, *41*, 1227.

(35) Zhang, Z.; Verykios, X. E. Mechanistic Aspects of Carbon Dioxide Reforming of Methane to Synthesis Gas over Ni Catalysts. *Catal. Today* **1994**, *21*, 589.

(36) Olsbye, U.; Wurzel, T.; Mleczko, L. Kinetic and Reaction Engineering Studies of Dry Reforming of Methane over a Ni/La/Al_2O_3 Catalyst. *Ind. Eng. Chem. Res.* **1997**, *36*, 5180.

(37) Osaki, T.; Horiuchi, T.; Suzuki, K.; Mori, T. *Appl. Catal. A* **1997**, *155*, 229.

(38) Kroll, V. C. H.; Tjatjopoulos, G. J.; Mirodatos, C. Kinetics of Methane Reforming over Ni/SiO_2 Catalysts Based on a Stepwise Mechanistic Model. *Stud. Surf. Sci. Catal.* **1998**, *119*, 753.

(39) Wang, S.; Lu, G. Q. Reaction Kinetics and Deactivation of Ni-based Catalysts in CO_2 Reforming of Methane. *React. Eng. Pollut. Prev.* **2000**, 75.

(40) Iyer, M. V. New Catalysts for Syngas Production from Carbon Dioxide and Methane. M.S.Ch.E. Thesis, West Virginia University, Morgantown, WV, 2001.

(41) Liu, Z.; Li, X.; Close, M. R.; Kugler, E. L.; Peterson, J. L.; Dadyburjor, D. B. Screening of Alkali-Promoted Vapor-Phase-Synthesized Molybdenum Sulfide Catalysts for the Production of Alcohols from Synthesis Gas. *Ind. Eng. Chem. Res.* **1997**, *36* (8), 3085.

(42) Tsuji, M.; Miyao, T.; Naito, S. Remarkable Support Effect of ZrO_2 upon the CO_2 Reforming of CH_4 over Supported Molybdenum Carbide Catalysts. *Catal. Lett.* **2000**, *69*, 195.

(43) Wang, S.; Lu, G. Q. Effects of Acidic Treatments on the Pore and Surface Properties of Ni Catalyst Supported on Activated Carbon. *Carbon* **1998**, *35*, 283.

(44) Sandler, S. I. *Chemical Engineering Thermodynamics*, 2nd ed.; John Wiley & Sons: New York, 1989.

(45) Vannice, M. A.; Hyun, S. H.; Kalpakci, B.; Liauh, W. C. Entropies of Adsorption in Heterogeneous Catalytic Reactions. *J. Catal.* **1979**, *56*, 358.

(46) Lee, H. H. *Heterogeneous Reactor Design*; Butterworth Publishers: Stoneham, MA, 1985.

Received for review August 28, 2002
Revised manuscript received January 15, 2003
Accepted March 7, 2003

IE020677Q